Published in final edited form as:
Matrix Biol. 2010 September ; 29(7): 621–628. doi:10.1016/j.matbio.2010.06.005.

MECHANISMS OF EMPHYSEMA IN AUTOSOMAL DOMINANT CUTIS LAXA

Qirui Hu[a], **Adrian Shifren**[b], **Carla Sens**[a], **Jiwon Choi**[c], **Zoltan Szabo**[a], **Barry C. Starcher**[d], **Russell H. Knutsen**[e], **J. Michael Shipley**[b], **Elaine C. Davis**[c], **Robert P. Mecham**[e], and **Zsolt Urban**[a,b,f,*]

[a]Department of Pediatrics, Washington University School of Medicine, St. Louis, MO, 63110, USA

[b]Department of Medicine, Washington University School of Medicine, St. Louis, MO, 63110, USA

[c]Department of Anatomy and Cell Biology, McGill University, Montreal, QC, H3A 2B2, Canada

[d]Department of Biochemistry, University of Texas Health Center, Tyler, TX, 75708, USA

[e]Department of Cell Biology and Physiology, Washington University School of Medicine, St. Louis, MO, 63110, USA

[f]Department of Human Genetics, Graduate School of Public Health, University of Pittsburgh, Pittsburgh, PA 15261, USA

Abstract

Heterozygous elastin gene mutations cause autosomal dominant cutis laxa associated with emphysema and aortic aneurysms. To investigate the molecular mechanisms leading to cutis laxa *in vivo*, we generated transgenic mice by pronuclear injection of minigenes encoding normal human tropoelastin (WT) or tropoelastin with a cutis laxa mutation (CL). Three independent founder lines of CL mice showed emphysematous pulmonary airspace enlargement. No consistent dermatological or cardiovascular pathologies were observed. One CL and one WT line were selected for detailed studies. Both mutant and control transgenic animals showed elastin deposition into pulmonary elastic fibers, indicated by increased desmosine levels in the lung and by colocalization of transgenic and endogenous elastin by immunostaining. CL mice showed increased static lung compliance and decreased stiffness of lung tissue. In addition, markers of transforming growth factor-β (TGFβ) signaling and the unfolded protein response (UPR) were elevated together with increased apoptosis in the lungs of CL animals. We conclude that the synthesis of mutant elastin in CL activates multiple downstream disease pathways by triggering a UPR, altered mechanical signaling, increased release of TGFβ and apoptosis. We propose that the combined effects of these processes lead to the development of an emphysematous pulmonary phenotype in CL.

[*]**Corresponding author:** Zsolt Urban, Ph.D., Department of Human Genetics, 130 DeSoto Street, A300 Crabtree Hall, Pittsburgh, PA 15261, USA, Phone: +1-412-648-8269, Fax: +1-412-624-3020, urbanz@pitt.edu.

Conflict of interest statement
The authors declare no conflict of interest.

Keywords

chronic obstructive pulmonary disease; mutation; elastin; growth factor; unfolded protein response; transgenic mouse

1. Introduction

Elastic fibers are extracellular matrix (ECM) structures consisting of fibrillin microfibrils, elastin and a considerable number of associated proteins. They are responsible for the resilience of tissues which are subjected to repeated extension by facilitating spontaneous and efficient recoil (Kielty, 2006). In addition to providing structural and mechanical support, elastic fibers provide key developmental signals in the terminal differentiation of vascular smooth muscle cells (Karnik et al., 2003). Furthermore, fibrillin microfibrils are necessary for the regulation of the bioavailablility of several growth factors, including transforming growth factor-β (TGFβ) (Neptune et al., 2003) and bone morphogenetic protein (BMP) 2, BMP4 and BMP7 (Sengle et al., 2008). The assembly of elastic fibers is a complex, stepwise, dynamic and cell directed process through which microaggregates of the elastin precursor, tropoelastin, are deposited onto a preformed template of microfibrils, which then undergo a series of maturation steps (Wagenseil and Mecham, 2007).

Consistent with the essential role of elastin in the development and homeostasis of multiple tissues, heterozygous mutations in the elastin gene (*ELN*) can cause two distinct autosomal dominant inherited disorders. Loss of function mutations in *ELN* lead to supravalvular aortic stenosis (MIM 185500), a cardiovascular disease characterized primarily by obstructive lesions in the aorta and other great arteries [reviewed in (Pober et al., 2008)]. A different set of mutations in *ELN* result in autosomal dominant cutis laxa (ADCL, MIM 123700), a syndrome of loose, redundant and inelastic skin associated with variable musculoskeletal [hernia (Szabo et al., 2006; Tassabehji et al., 1998; Zhang et al., 1999)], cardiovascular [aortic aneurysm (Szabo et al., 2006), (Callewaert *et al.,* submitted), peripheral pulmonary artery stenosis (Tassabehji et al., 1998)], and pulmonary [bronchiectasis, emphysema (Rodriguez-Revenga et al., 2004; Urban et al., 2005)] involvement.

The most common molecular defects in ADCL are frameshift mutations located in exons 30, 32 and 33 at the 3'-end of *ELN* (Rodriguez-Revenga et al., 2004; Szabo et al., 2006; Tassabehji et al., 1998; Zhang et al., 1999), (Callewaert *et al.,* submitted). Naturally occurring alternative splicing of exon 32 and mutation-induced exon skipping can lead to multiple mutant transcripts in ADCL cells, complicating the analysis of the molecular consequences of these mutations. However, a common shared feature of mutant transcripts in ADCL is the replacement of the authentic C-terminus of the encoded tropoelastin molecule with a missense peptide sequence of variable length (Szabo et al., 2006; Tassabehji et al., 1998; Zhang et al., 1999) (*Callewaert et al.,* submitted). Several *in vitro* studies have shown that mutant tropoelastin in ADCL is secreted and incorporated into the ECM, albeit with reduced efficiency (Tassabehji et al., 1998; Urban et al., 2005). Whereas the proximal consequences of ADCL mutations are beginning to emerge, the downstream molecular signals that lead to the development of ADCL are unknown.

In light of previous data, we hypothesized that a dominant negative mechanism may be the basis of ADCL. To test this hypothesis, we generated transgenic mouse lines that expressed human ADCL mutant elastin on a normal mouse genetic background. Mutant transgenic animals had lung disease ranging from airspace enlargement to severe emphysema. In contrast, transgenic expression of wild-type human elastin produced no significant change in lung physiology. Furthermore, we show that emphysematous disease in CL mice is

associated with altered lung mechanics, increased TGFβ signaling, activation of the UPR and increased apoptosis. These findings show that elastin mutations can indeed act in a dominant manner to cause CL-like pulmonary lesions *in vivo,* and establish a connection between the mechanical properties of tissues, growth factor signaling and cell survival.

2. Results

2.1. A transgenic mouse model of autosomal dominant cutis laxa

We previously identified *ELN* mutation c.2114_2138del in a family with ADCL, hernias, aortic aneurysms and pulmonary air trapping (Szabo et al., 2006). We showed that this 25 base pair deletion, located in exon 30, resulted in the synthesis of multiple mutant transcripts. The most abundant of these mRNA species lacked the sequence encoded by exon 32 as a result of normal alternative splicing and, following the reading frame shift caused by the deletion, coded for an 81 amino acid long C-terminal missense peptide sequence corresponding to exons 30, 31, 33, 34 and part of the 3'-untraslated region of *ELN*. We used the cDNA for this mutant transcript as a basis of our transgene (Fig. 1). In addition, to permit rapid monitoring of transgene expression at the protein level, we included the coding region for enhanced green fluorescent protein (EGFP) as a second cistron following an internal ribosomal entry site. As a control, we generated a transgene to express a common normal isoform of human tropoelastin, lacking exons 22, 26A and 32, a wild-type counterpart of our mutant construct.

Because the transcriptional regulation of the elastin gene is incompletely characterized, we have used a recombinant regulatory region to express our transgenes (Fig. 1). This upstream sequence, consisting of a cytomegalovirus immediate early enhancer and a chicken beta actin promoter was a derivative of the pCX-GFP expression vector (Ikawa et al., 1995) and has been shown to be ubiquitously active in transgenic mouse experiments (Okabe et al., 1997).

Transgenic mice were generated using pronuclear injection of minigenes containing either a human elastin cDNA with a cutis laxa mutation 2114_2138del (CL) or a wild-type human elastin cDNA (WT). Several transgenic founder lines were identified by PCR screening of genomic DNA. Transgene expression was confirmed by RT-PCR and immunoblotting analysis (not shown). We also used EGFP for direct visual and stereomicroscopic observation of transgene expression. These analyses showed ubiquitous, high expression of the transgene in most lines and tissues (data not shown). Based on these preliminary studies, three CL founder lines (2, 51 and 60) and one WT line were selected for further investigation.

2.2. Emphysematous lung disease in CL mice

Detailed gross anatomical and histological evaluation of CL mice revealed no consistent abnormalities in the skin and blood vessels. In contrast, line 2 CL mice showed severe respiratory distress, smaller size and significant mortality with an average survival of 47 days and a range of 7–89 days (n=16). To investigate if pulmonary disease is a shared characteristic of CL mice, we subjected all transgenic lines and nontrangenic (NTg) controls to histological evaluation of lung tissue inflated to a standard pressure (20 cm H_2O). No significant alteration of lung architecture was found in WT transgenic mice (Fig. 2B) compared to NTg controls (Fig. 2A). Conversely, line 2 CL lungs showed severe emphysema (Fig. 2C). Moreover, both line 51 (Fig. 2D) and line 60 (Fig. 2E) CL lungs had enlarged alveoli. Quantitative morphometry confirmed significant airspace enlargement in all CL lines and normal alveolar sizes in WT transgenic mice (Fig. 2F).

Because of significant lethality, line 2 CL could not be maintained and therefore was not available for detailed experimentation. As both line 51 CL and line 60 CL showed similar airspace enlargement, only one of these lines, line 60 CL, was used for subsequent, detailed functional studies along with WT and NTg controls. In the rest of the study, line 60 CL is simply referred to as CL.

2.3. Synthesis and incorporation of transgenic elastin into elastic fibers

To determine transgene mRNA expression levels, real-time RT-PCR using absolute quantification was applied, normalized to 18S ribosomal RNA abundance as a loading control. Transgene expression was comparable in the lungs of WT controls and CL mice (Fig. 3A). To explore the localization of transgenic elastin relative to endogenous mouse elastin, we performed immunofluorescent staining of lung sections utilizing a human-specific monoclonal antibody and a mouse-specific polyclonal anti-elastin antibody (Fig. 3B). As expected, lungs from NTg animals were negative for the human-specific antibody, whereas strong mouse elastin staining was observed. Both WT and CL transgenic animals showed strong colocalization of mouse and human elastins, thus demonstrating that transgenic and endogenous elastins can contribute to the same elastic fiber network. Whereas WT elastin was mainly localized to the ECM, considerable intracellular elastin staining was observed in CL lungs (Fig. 3B, arrowheads), suggesting that the secretion of mutant elastin was less efficient than the secretion of WT elastin.

To study the tissue specificity of the disease phenotype in our mouse model, we stained skin and aortic sections for mouse and human elastin. Whereas WT transgenic elastin was incorporated into the elastic fibers in these tissues, no staining was detectable for mutant elastin in the ECM of CL animals in skin and aorta (data not shown). This finding, combined with the lack of skin and aortic phenotype in the CL mice indicates that incorporation of mutant elastin into elastic fibers is necessary for the development of CL-related disease.

To investigate the combined effect of endogenous and transgenic elastin expression on elastic fiber formation, we measured the levels of desmosine, a crosslinking amino acid specific for mature elastin, in lung samples. Lung samples from both CL and WT mice contained significantly ($p<0.001$) higher amounts of desmosine than NTg mice (Fig. 3). These results show that transgenic elastin not only colocalizes with endogenous elastic fibers but also contributes to mature, crosslinked elastin.

2.4. CL elastin markedly alters lung mechanics

To explain the observation of increased airspace CL mice, we evaluated the mechanical properties of the lungs. Expiratory static pressure-volume curves of CL lungs were shifted to the left compared with NTg controls, indicating that lung elastic recoil pressure in CL mice was reduced (Fig. 4A). Static compliance measurements, calculated from the slopes of the curves, indicated that at all lung volumes, CL lungs had greater compliance than NTg lungs. In contrast, elastic recoil pressures and lung compliance of WT lungs were almost identical to those of NTg lungs. Calculation of specific lung compliance at functional residual capacity (FRC) ~ 0.25ml (Lai and Chou, 2000) showed lung compliance for NTg = 0.06ml/cmH_2O, WT = 0.06ml/cmH_2O, and CL = 0.07ml/cmH_2O, with only the difference between NTg and CL mice being statistically significant ($p=0.015$).

Stress-strain curves of isolated lung tissue strips from NTg, WT and CL lungs were recorded at amplitudes approximating those experienced during tidal volume breathing at functional residual capacity (FRC) (Fig. 4B). The net effect of CL mutant elastin in the lung was a shift in the stress-strain curve to the right. Calculation of the incremental elastic modulus (a

measure of lung tissue stiffness) at intermediate strains revealed that NTg tissue stiffness (9.58N/cm^2) was significantly greater than that of CL lung tissue (5.75N/cm^2) (p=0.005), but almost identical to WT lung tissue (9.47N/cm^2) (p=0.83). Thus, the elastic modulus (stiffness) of lung tissue decreased when CL mutant elastin was incorporated into lung elastic fibers, but not when normal human elastin was present.

2.5. Increased TGFβ signaling, ER stress and apoptosis in CL mice

Recent studies indicate that mechanical forces are involved in the release of latent TGFβ from the ECM (Wipff et al., 2007). To test if altered lung mechanics may impact TGFβ activity in our model, we stained lung sections for pSMAD2, a marker of TGFβ signaling (Fig. 5A). Quantitative evaluation of pSMAD2-positive nuclei showed a highly significant increase in the lungs of CL mice, whereas WT mice showed no difference compared to NTg (Fig. 5B).

Both previous studies on cultured fibroblasts from patients with ADCL (Urban et al., 2005) and our current observation of intracellular protein retention (Fig. 3B) suggest that CL mutations interfere with efficient secretion of tropoelastin. Missense residues in mutant proteins often lead to misfolding and retention of the protein in the ER (Schroder and Kaufman, 2005). Concomitantly, a signaling cascade, the UPR, is elaborated which results in the suppression of translation and increased production of chaperones. A key molecule in this pathway is the eukaryotic initiation factor 2α (eIF2a) whose phosphorylation is a sensitive and specific marker of the UPR. To test if synthesis of CL mutant tropoelastin triggers ER stress, we stained lung sections for transgenic elastin and phosphorylated eIFa (peIF2a) (Fig. 5C). In CL lungs, the frequency of peIF2a positive cells was significantly elevated (Fig. 5D). Importantly, 80% of the peIF2a positive cells were also positive for CL elastin (Fig. 5C, arrows) suggesting that retention of mutant tropoelastin and activation of the UPR occurred in the same cells. Expression of WT human tropoelastin, in contrast, did not result in UPR activation compared to NTg mice (Fig. 5D).

Elevated TGFβ signaling often leads to apoptosis of epithelial (Lee et al., 2006), endothelial (Pollman et al., 1999) and hematopoetic cell lineages (Licona-Limon and Soldevila, 2007). It is also known that persistent activation of the UPR is a potent pro-apoptotic signal (Schroder and Kaufman, 2005). Therefore, we studied apoptosis in CL mice by terminal deoxynucleotidyl transferase-mediated deoxyuridine triphosphate nick end-labeling (TUNEL) staining (Fig. 5E). Both NTg and WT mice showed consistently very low apoptosis index ranging 0.001–0.002. The apoptosis index in CL mouse lungs remained low in absolute terms (0.005) but was significantly elevated compared to NTg mice (Fig. 5F).

3. Discussion

Early clinical studies suggested that ADCL is a benign skin disease with few systemic lesions (Beighton, 1972). However, subsequent reports have shown that emphysema (Kelleher et al., 2005; Rodriguez-Revenga et al., 2004; Urban et al., 2005) and aortic aneurysms (Szabo et al., 2006) were also part of the phenotypic profile of this syndrome and can lead to significant morbidity and mortality. Our results show that overexpression of mutant elastin on the normal murine background recapitulates the pulmonary phenotype associated with ADCL ranging from mild airspace enlargement to severe emphysema and respiratory failure. In contrast, overexpression of wildtype human elastin resulted in no detectable disease.

Despite ubiquitous expression of the transgenes, histological evaluation showed appropriate distribution of elastic fibers in transgenic animals indicating that the regulated expression of other elastic fiber components such as fibrillins, fibulins and lysyl oxidases was sufficient to

direct normal patterning of both endogenous and transgenic elastin. These studies provide the first *in vivo* evidence that mutant tropoelastin in CL can copolymerize with WT elastin providing a molecular mechanism for the dominant negative action of CL mutations. The notion that copolymerization of mutant and normal elastin is required for this dominant negative disease mechanism is further supported by the observation that skin and aorta where CL elastin was not incorporated into elastic fibers were unaffected in our mice.

Although the quantity and distribution of elastic fibers in mutant and control lungs were similar, mechanical studies indicated that elastic fibers containing mutant elastin were functionally impaired. Pressure-volume analysis at volumes approximating FRC in mice showed that CL lungs had significantly greater compliance than NTg animals. Because WT lung compliance was essentially identical to that of NTg lungs, these results suggest that mutant elastin critically affects lung mechanical properties. To control for the effects of surface tension on lung mechanics, the air-liquid interface, critical for surfactant function, was eliminated by measuring the mechanics of isolated lung tissue strips in a tissue bath. This allowed for accurate determination of the role of the ECM in lung mechanics. To ensure the physiologic relevance of our results, we utilized stress and strain amplitudes approximating the range experienced during tidal volume breathing around FRC. Our data demonstrate that pulmonary elastin quality contributes to lung tissue elasticity across the range of strains experienced around FRC. The decreased tissue stiffness demonstrated by CL mutant elastin tissue should result in greater lung compliance, a finding confirmed by the static compliance measurements. Notably, these data were comparable to our previous work showing that reduced elastin content had similar effects on lung compliance (Shifren et al., 2007). This suggests that inclusion of CL mutant elastin with normal elastin into the same elastic fibers results in a copolymer that is functionally similar to reduced quantities of normal elastin with respect to pulmonary mechanical function, a dominant negative mechanism.

The observation that WT lungs demonstrated similar tissue stiffness to NTg lungs and likewise similar compliance shows that normal splice isoforms of human elastin behave in a manner similar to wild-type mouse elastin with respect to mechanical function. Demosine measurements showed increased elastin content in WT lungs compared to NTg. The observation that WT mice did not have altered lung compliance despite having more elastin is surprising, as one would expect increased stiffness in the presence of more, functional elastin. We can only speculate that the pulmonary elastic fiber network is organized in a way that makes lung compliance relatively resistant to fluctuations in elastin content within a certain window. Previous studies showed significant increase in lung compliance in the presence of a 50% reduction in elastin content (Shifren et al., 2007) constraining the proposed window of elastin amount compatible with normal mechanical function. Here we show that a doubling lung elastin is compatible with normal mechanics. This has important implications for the treatment of elastin-related lung disease such as emphysema, as over-expression of elastin appears to be an approach with no adverse effects on lung mechanics.

Concomitant with altered pulmonary mechanics, expression of the CL mutant elastin was also associated with enhanced TGFβ signaling. Recent studies show that myofibroblast contraction or stretching of the ECM can result in a rapid release of latent TGFβ (Wipff et al., 2007) *in vitro*. Altered pulmonary mechanics in our CL model results in increased extension of the lung parenchyma at normal respiratory pressure gradients that may lead to increased release of TGFβ from ECM stores resulting in the observed elevation in the number of pSMAD2 positive cells. Concomitant studies on cells form ADCL patients with elastin gene mutations have also found evidence of increased TGFβ signaling (Callewaert *et al.,* submitted). Therefore, we conclude that enhanced TGFβ signaling is a part of the CL disease mechanism independent of the model system used.

Several lines of evidence support the possibility of a specific toxic effect of mutant proteins associated with cutis laxa. Most elastin mutations associated with ADCL involve a C-terminal −1 frameshift, leading to the replacement of the normal C-terminus with similar missense peptide sequences (Rodriguez-Revenga et al., 2004; Szabo et al., 2006; Tassabehji et al., 1998; Zhang et al., 1999). These sequences in turn may disrupt trafficking of tropoelastin and lead to the activation of the UPR and cell death pathways. Consistent with this notion, increased intracellular immunostaining for mutant tropoelastin (Urban et al., 2005), activation of UPR markers and increased apoptosis (Callewaert *et al.,* submitted) were observed in skin fibroblasts from patients with ADCL, especially if the mutation was a −1 frameshift, located in exon 30. We show that UPR activation and increased cell death is also occurs in an *in vivo* model of ADCL.

Recent investigations of missense fibulin-5 mutations associated with recessive cutis laxa and lethal infantile emphysema showed increased ER stress and increased apoptosis in mutant fibroblasts, providing further evidence for the contribution of misfolded protein-related toxicity to the pathogenesis of emphysema in cutis laxa (Hu et al., 2006). Together with the present report, these findings support the recently recognized idea that dysregulation of growth factor signaling pathways and activation of cell death pathways are key mechanisms in the development of emphysema (Kasahara et al., 2000; Ma et al., 2005; Petrache et al., 2006; Petrache et al., 2005), and raise the possibility that targeting these mechanisms may lead to effective treatments of emphysematous disease both in the context of cutis laxa and in more common forms of chronic obstructive pulmonary disease.

4. Experimental Procedures

4.1. Transgenic constructs

As a parental construct, plasmid pIBR2 (a kind gift of Dr. Stefan Moisyadi, University of Hawaii), generated from pCX-GFP by replacing the green fluorescent protein cassette with a fragment containing an internal ribosomal entry site and an EGFP cDNA was used. Wildtype and mutant elastin cDNAs were isolated by RT-PCR cloning from RNA isolated from wildtype and mutant human fibroblasts and were confirmed by direct DNA sequencing prior to insertion into the pIBR2 plasmid.

4.2. Generation of transgenic animals

Plasmid DNA was purified using an EndoFree Plasmid Maxi kit (Qiagen, Valencia, CA), digested with AseI and SspI restriction enzymes, and the minigene fragment was separated from the plasmid by agarose gel electrophoresis. Linear minigene DNA was recovered using a QIAEX II kit (Qiagen) and diluted to a concentration of 2ng/ul using injection buffer. DNA was injected into fertilized C57Bl/6J eggs, and then implanted into pseudo-pregnant foster animals. Founder animals were identified using a previously published PCR method that detects an EGFP sequence from the transgene and a fatty acid-binding protein (Fabpi) sequence as an internal positive control (Stratman et al., 2003). Transgenic lines were maintained as heterozygotes by breeding to wildtype C57Bl/6J mice.

4.3. Analysis of transgene expression

To quantify expression of the transgene or the endogenous mouse elastin gene, real-time RT-PCR was used. Skin, lung and aorta were harvested at postnatal day 21. Total RNA was isolated using a VERSAGENE Total RNA Purification Kit (Gentra, Minneapolis, MN). Reverse transcriptions (RT) were performed using SuperScript III First-Strand Synthesis System (Invitrogen, Carlsbad, CA). PCR amplification was performed with a primer set flanking either the chick beta-actin intron within the transgene (5’-AGTCGCTGCGTTGCCTTC-3’ and 5’-CAGCACAACAACCAGCACGT-3’) or intron 22

of the endogenous mouse elastin gene (5'-GCCGCCAAAGCTRGCTAAAGTA-3' and 5'-GGCACAGCTGGTACTGCAC-3'), each amplification generating a product of 99 bp. RT-PCR products were amplified twice using the same primers as used for real-time RT-PCR and were retrieved from the agarose gel. The concentration of RT-PCR products was measured using UV spectrometry, and copy number was calculated. A series of standards were prepared by dilution and used as templates to generate standard curves of real-time RT-PCR. Final results were normalized to the copy number of 18S ribosomal RNA in same tissue.

4.4. Desmosine measurements

Desmosine analysis was performed on single lobes of mouse lungs. The tissues were placed in microfuge tubes and hydrolyzed in 500 μl of 6N HCl at 105°C for 24 h. The hydrolysates were evaporated to dryness, re-dissolved in water and assayed for desmosine by RIA as described previously (Starcher and Conrad, 1995). The protein content of the tissue hydrolysate was determined by a ninhydrin-based method as described (Starcher, 2001).

4.5. Histology and quantitative morphometry

Lungs were inflated with 4% paraformaldehyde in phosphate-buffered saline at a pressure of 20 cm H_2O through the trachea. Inflated lungs were removed and further fixed in 4% paraformaldehyde for 2 days. After embedding in paraffin, 5 μm-thick sections were cut, deparaffinized in Histo-Clear (National Diagnostics, Atlanta, GA) and then rehydrated. All histological sections were stained with hematoxylin-eosin staining and Hart's stain for elastin, as described previously (Hucthagowder et al., 2006). For chord length measurement, hematoxylineosin sections were utilized. Ten fields at 10× magnification were captured randomly from each section using an Axioskop BX60 microscope (Olympus, Center Valley, PA). Chord length analysis was performed using NIH Image software (Version 1.63, NIH, Bethesda, MD) with a chord length macro (available at http://rsb.info.nih.gov/nih-image). Binarized, inverted lung micrographs were manually thresholded, and subjected to a logical "AND" operation with horizontal and vertical grids of parallel lines. The line lengths overlying alveolar spaces were measured and averaged to yield mean chord length. Chord lines touching the edges of the image fields were excluded from analysis to ensure that mean chord length included only line segments overlapping alveolar walls at both ends. Chord length measurement was chosen over mean linear intercept as it has the advantage of being independent of alveolar septal thickness. Each group analyzed contained 4 animals.

4.6. Immunostaining

Lung sections were deparaffinized and rehydrated. Antigen retrieval was performed by microwaving sections in 0.1 M citrate buffer (pH 6.0) for 5 min three times at 350 W or by treating the sections with 20 μg/ml Proteinase K. Autofluorescence was blocked by incubating the sections in 100 mM $CuSO_4$ for 15 min. After blocking with 1.5% normal serum for 1 h, sections were incubated with primary antibody at 4°C overnight. Mouse and human elastins were detected using a polyclonal (MRT6-17) (Kozel et al., 2003) or a monoclonal (MAB2503, Chemicon, Temecula, CA) antibody, respectively. Signaling molecules pSMAD2 and peIF2a were detected by polyclonal antibodies (Cell Signaling Technology, Danvers, MA). Primary antibodies were followed by incubation with fluorophore-conjugated (AlexaFluor 488 and AlexaFluor 594) secondary antibodies (Invitrogen). Nuclei were stained using Hoechst 33258 dye (Sigma, St. Louis, MO). Sections were mounted with Gel/Mount (Biomeda, Burlingame, CA), and were visualized with an Axioskop BX60 microscope (Olympus). For quantification of pSMAD2 and peIF2a staining, 10 images were taken randomly from each section. Each experimental group contained 4 animals with 1 section per animal.

Apoptotic cells were visualized using an *In situ* Cell Death Detection Kit, Fluorescein (Roche Applied Science, Indianapolis, IN) based on a terminal deoxynucleotidyl transferase-mediated deoxyuridine triphosphate nick end-labeling (TUNEL) method. Lung sections were deparaffinized, rehydrated and treated with 350 W microwave irradiation for 5 minutes in 0.1 M citrate buffer (pH 6.0). Label solution and enzyme solution were mixed at a ratio of 2:1. Each section was covered with 50 μl TUNEL reaction mixture. Slides were incubated in a humidified chamber for 1 h at 37°C. After several washes, nuclei were stained using propidium iodide (Sigma). Sections were mounted with Gel/Mount (Biomeda), and were visualized with an Axioskop BX60 microscope (Olympus). For quantitative analysis, 5 images were taken randomly from each section. Each experimental group contained 4 animals with 1 section per animal.

4.7. Static lung compliance assessment

Three-month-old mice from all three genotypes were euthanized with sodium pentobarbital and the tracheas cannulated through a neck incision. Lungs were removed *en bloc* with the cannula *in situ* and placed in a humidity chamber to avoid desiccation. The cannula was connected via a three-way stopcock system to a graduated syringe and a modified pressure arteriograph (Pressure Myograph System P-100, Danish Myotechnology, Copenhagen, Denmark) as used previously (Faury et al., 2003; Wagenseil et al., 2005). Starting at residual volume (no inflation, trachea open to atmospheric pressure), the lungs were inflated in 0.1 ml increments every 30 sec to a maximum volume of 1.2 ml (total lung capacity in C57Bl/6J mice ~1.0 ml) (Irvin and Bates, 2003). Pressure and volume on inflation were recorded using Myoview Acquisition software (Danish Myotechnology) to produce a static pressure-volume curve. Expiratory curves are represented. Static compliance was determined by calculating the slope of the expiratory curve at functional residual volume (approximately 0.25 ml) (Salazar and Knowles, 1964). Each group analyzed contained a minimum of 5 animals.

4.8. Stress-strain measurements

Three-month-old mice from all three genotypes were euthanized with sodium pentobarbital. The lungs were removed, placed into balanced physiologic saline (130 mM NaCl, 15 mM $NaHCO_3$, 5.5 mM dextrose, 4.7 mM KCl, 1.2 mM $MgSO_4 \cdot 7H_2O$, 1.2 mM KH_2PO_4, 0.026 mM EDTA, and 1.6 mM $CaCl_2$, pH 7.2) on ice, and separated into individual lobes. Lung parenchymal strips were obtained by cutting tissue strips from the long axis of each lobe. The tissue strips were fixed to adjustable metal posts mounted on a force transducer (Danish Myotechnology). A central region along the attached tissue strip length was chosen for diameter and length measurements. Tissue strip length was adjusted manually using a micrometer attached to one of the metal posts. The starting length and cross-sectional area for each strip was determined as the inter-post distance after three preconditioning cycles from 0 to 0.1 mm. At the starting length, the force was set to zero and the strips were stretched from 0 to 0.4 mm (or until yield strength was exceeded) in steps of 20 μm for 45 sec per step to allow for force equilibration at each new length. At 45 sec the force was recorded. All measurements were performed in a heated tissue bath containing balanced physiologic saline at 37° C within 1 h of sacrifice. The length and force measurements were normalized to obtain stress (σ) and stretch ratio (λ) as $\sigma = F/Ao$; $\lambda = [l + lo]/lo$ where l is stretched length, lo is starting length of the strip, F is measured force, and Ao is cross-sectional area of the strip corresponding to lo. The elastic modulus (Y) of each tissue was calculated by determining the slope of the stress-strain curves over changes in measured length (l). Each group analyzed contained a minimum of 5 animals and utilized at least 1 strip per lobe from each animal.

Acknowledgments

We thank Dr. Yusuke Marikawa, Sandra E. Dunn, and Stefanie Lerche for technical help with the early stages of this project, Ron McCarthy in the Pulmonary and Critical Care Division's transgenic mouse core for microinjections of transgenic constructs, Dr. Richard A. Pierce for advice on immunostaining, Dr. Louis J. Muglia and Dr. David B. Wilson for critical reading of the manuscript. This study was funded by the National Institutes of Health/National Heart Lung and Blood Institute (HL073703 to Z.U., HL084922 to Z.U. and R.P.M.) and the Canadian Institutes of Health Research (MOP86713 to E.C.D.); Canada Research Chair (to E.C.D.).

References

Beighton P. The dominant and recessive forms of cutis laxa. J Med Genet. 1972; 9:216–221. [PubMed: 5046633]

Faury G, Pezet M, Knutsen RH, Boyle WA, Heximer SP, McLean SE, Minkes RK, Blumer KJ, Kovacs A, Kelly DP, Li DY, Starcher B, Mecham RP. Developmental adaptation of the mouse cardiovascular system to elastin haploinsufficiency. J Clin Invest. 2003; 112:1419–1428. [PubMed: 14597767]

Hu Q, Loeys BL, Coucke PJ, De Paepe A, Mecham RP, Choi J, Davis EC, Urban Z. Fibulin-5 mutations: mechanisms of impaired elastic fiber formation in recessive cutis laxa. Hum Mol Genet. 2006; 15:3379–3386. [PubMed: 17035250]

Hucthagowder V, Sausgruber N, Kim KH, Angle B, Marmorstein LY, Urban Z. Fibulin-4: a novel gene for an autosomal recessive cutis laxa syndrome. Am J Hum Genet. 2006; 78:1075–1080. [PubMed: 16685658]

Ikawa M, Kominami K, Yoshimura Y, Tanaka K, Nishimune Y, Okabe M. A rapid and non-invasive selection of transgenic embryos before implantation using green fluorescent protein (GFP). FEBS Lett. 1995; 375:125–128. [PubMed: 7498460]

Irvin CG, Bates JH. Measuring the lung function in the mouse: the challenge of size. Respir Res. 2003; 4:4. [PubMed: 12783622]

Karnik SK, Brooke BS, Bayes-Genis A, Sorensen L, Wythe JD, Schwartz RS, Keating MT, Li DY. A critical role for elastin signaling in vascular morphogenesis and disease. Development. 2003; 130:411–423. [PubMed: 12466207]

Kasahara Y, Tuder RM, Taraseviciene-Stewart L, Le Cras TD, Abman S, Hirth PK, Waltenberger J, Voelkel NF. Inhibition of VEGF receptors causes lung cell apoptosis and emphysema. J Clin Invest. 2000; 106:1311–1319. [PubMed: 11104784]

Kelleher CM, Silverman EK, Broekelmann T, Litonjua AA, Hernandez M, Sylvia JS, Stoler J, Reilly JJ, Chapman HA, Speizer FE, Weiss ST, Mecham RP, Raby BA. A functional mutation in the terminal exon of elastin in severe, early-onset chronic obstructive pulmonary disease. Am J Respir Cell Mol Biol. 2005; 33:355–362. [PubMed: 16081882]

Kielty CM. Elastic fibres in health and disease. Expert Rev Mol Med. 2006; 8:1–23. [PubMed: 16893474]

Kozel BA, Wachi H, Davis EC, Mecham RP. Domains in tropoelastin that mediate elastin deposition in vitro and in vivo. J Biol Chem. 2003; 278:18491–18498. [PubMed: 12626514]

Lai YL, Chou H. Respiratory mechanics and maximal expiratory flow in the anesthetized mouse. J Appl Physiol. 2000; 88:939–943. [PubMed: 10710389]

Lee CG, Kang HR, Homer RJ, Chupp G, Elias JA. Transgenic modeling of transforming growth factor-beta(1): role of apoptosis in fibrosis and alveolar remodeling. Proc Am Thorac Soc. 2006; 3:418–423. [PubMed: 16799085]

Licona-Limon P, Soldevila G. The role of TGF-beta superfamily during T cell development: new insights. Immunol Lett. 2007; 109:1–12. [PubMed: 17287030]

Ma B, Kang MJ, Lee CG, Chapoval S, Liu W, Chen Q, Coyle AJ, Lora JM, Picarella D, Homer RJ, Elias JA. Role of CCR5 in IFN-gamma-induced and cigarette smoke-induced emphysema. J Clin Invest. 2005; 115:3460–3472. [PubMed: 16284650]

Neptune ER, Frischmeyer PA, Arking DE, Myers L, Bunton TE, Gayraud B, Ramirez F, Sakai LY, Dietz HC. Dysregulation of TGF-beta activation contributes to pathogenesis in Marfan syndrome. Nat Genet. 2003; 33:407–411. [PubMed: 12598898]

Okabe M, Ikawa M, Kominami K, Nakanishi T, Nishimune Y. 'Green mice' as a source of ubiquitous green cells. FEBS Lett. 1997; 407:313–319. [PubMed: 9175875]

Petrache I, Fijalkowska I, Medler TR, Skirball J, Cruz P, Zhen L, Petrache HI, Flotte TR, Tuder RM. alpha-1 antitrypsin inhibits caspase-3 activity, preventing lung endothelial cell apoptosis. Am J Pathol. 2006; 169:1155–1166. [PubMed: 17003475]

Petrache I, Natarajan V, Zhen L, Medler TR, Richter AT, Cho C, Hubbard WC, Berdyshev EV, Tuder RM. Ceramide upregulation causes pulmonary cell apoptosis and emphysema-like disease in mice. Nat Med. 2005; 11:491–498. [PubMed: 15852018]

Pober BR, Johnson M, Urban Z. Mechanisms and treatment of cardiovascular disease in Williams-Beuren syndrome. J Clin Invest. 2008; 118:1606–1615. [PubMed: 18452001]

Pollman MJ, Naumovski L, Gibbons GH. Vascular cell apoptosis: cell type-specific modulation by transforming growth factor-beta1 in endothelial cells versus smooth muscle cells. Circulation. 1999; 99:2019–2026. [PubMed: 10209007]

Rodriguez-Revenga L, Iranzo P, Badenas C, Puig S, Carrio A, Mila M. A novel elastin gene mutation resulting in an autosomal dominant form of cutis laxa. Arch Dermatol. 2004; 140:1135–1139. [PubMed: 15381555]

Salazar E, Knowles JH. An Analysis of Pressure-Volume Characteristics of the Lungs. J Appl Physiol. 1964; 19:97–104. [PubMed: 14104296]

Schroder M, Kaufman RJ. ER stress and the unfolded protein response. Mutat Res. 2005; 569:29–63. [PubMed: 15603751]

Sengle G, Charbonneau NL, Ono RN, Sasaki T, Alvarez J, Keene DR, Bachinger HP, Sakai LY. Targeting of bone morphogenetic protein growth factor complexes to fibrillin. J Biol Chem. 2008; 283:13874–13888. [PubMed: 18339631]

Shifren A, Durmowicz AG, Knutsen RH, Hirano E, Mecham RP. Elastin protein levels are a vital modifier affecting normal lung development and susceptibility to emphysema. Am J Physiol Lung Cell Mol Physiol. 2007; 292:L778–L787. [PubMed: 17142349]

Starcher B. A ninhydrin-based assay to quantitate the total protein content of tissue samples. Anal Biochem. 2001; 292:125–129. [PubMed: 11319826]

Starcher B, Conrad M. A role for neutrophil elastase in the progression of solar elastosis. Connect Tissue Res. 1995; 31:133–140. [PubMed: 15612329]

Stratman JL, Barnes WM, Simon TC. Universal PCR genotyping assay that achieves single copy sensitivity with any primer pair. Transgenic Res. 2003; 12:521–522. [PubMed: 12885173]

Szabo Z, Crepeau MW, Mitchell AL, Stephan MJ, Puntel RA, Yin Loke K, Kirk RC, Urban Z. Aortic aneurysmal disease and cutis laxa caused by defects in the elastin gene. J Med Genet. 2006; 43:255–258. [PubMed: 16085695]

Tassabehji M, Metcalfe K, Hurst J, Ashcroft GS, Kielty C, Wilmot C, Donnai D, Read AP, Jones CJ. An elastin gene mutation producing abnormal tropoelastin and abnormal elastic fibres in a patient with autosomal dominant cutis laxa. Hum Mol Genet. 1998; 7:1021–1028. [PubMed: 9580666]

Urban Z, Gao J, Pope FM, Davis EC. Autosomal dominant cutis laxa with severe lung disease: synthesis and matrix deposition of mutant tropoelastin. J Invest Dermatol. 2005; 124:1193–1199. [PubMed: 15955094]

Wagenseil JE, Mecham RP. New insights into elastic fiber assembly. Birth Defects Res C Embryo Today. 2007; 81:229–240. [PubMed: 18228265]

Wagenseil JE, Nerurkar NL, Knutsen RH, Okamoto RJ, Li DY, Mecham RP. Effects of elastin haploinsufficiency on the mechanical behavior of mouse arteries. Am J Physiol Heart Circ Physiol. 2005; 289:H1209–H1217. [PubMed: 15863465]

Wipff PJ, Rifkin DB, Meister JJ, Hinz B. Myofibroblast contraction activates latent TGF-beta1 from the extracellular matrix. J Cell Biol. 2007; 179:1311–1323. [PubMed: 18086923]

Zhang MC, He L, Giro M, Yong SL, Tiller GE, Davidson JM. Cutis laxa arising from frameshift mutations in exon 30 of the elastin gene (ELN). J Biol Chem. 1999; 274:981–986. [PubMed: 9873040]

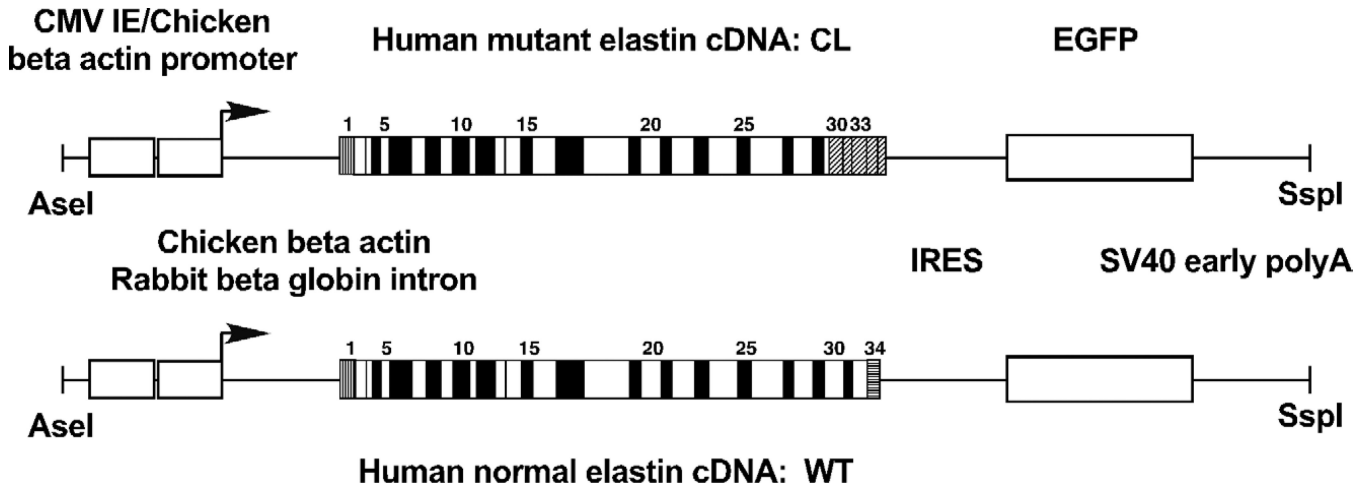

Figure 1. Transgenic constructs

Transcription of the transgenes was driven by a cytomegalovirus immediate-early enhancer (CMV IE) and a chicken beta actin promoter. Following the promoter, a hybrid intron was inserted consisting of chicken beta actin and rabbit beta globin sequences. The construct encoded a bicistronic mRNA consisting of either a mutant (CL) or a wild-type (WT) human elastin cDNA, an internal ribosomal entry site (IRES) and an enhanced green fluorescent protein (EGFP) cDNA. Each transgene concluded with a SV40 early viral polyadenylate addition site (polyA). The CL mutant cDNA was based on the major mutant mRNA isoform in a family with autosomal dominant cutis laxa caused by mutation 2114_2138del, located in exon 30 of the elastin gene. This frameshift mutation, in the absence of exon 32, which is frequently subject to removal by normally occurring alternative splicing, results in the replacement of the C-terminus of tropoelastin by a missense peptide sequence of 81 amino acids (oblique stripes). Because this mutant cDNA lacks the sequence corresponding to exon 32, the normal cDNA in our control transgenic construct also does.

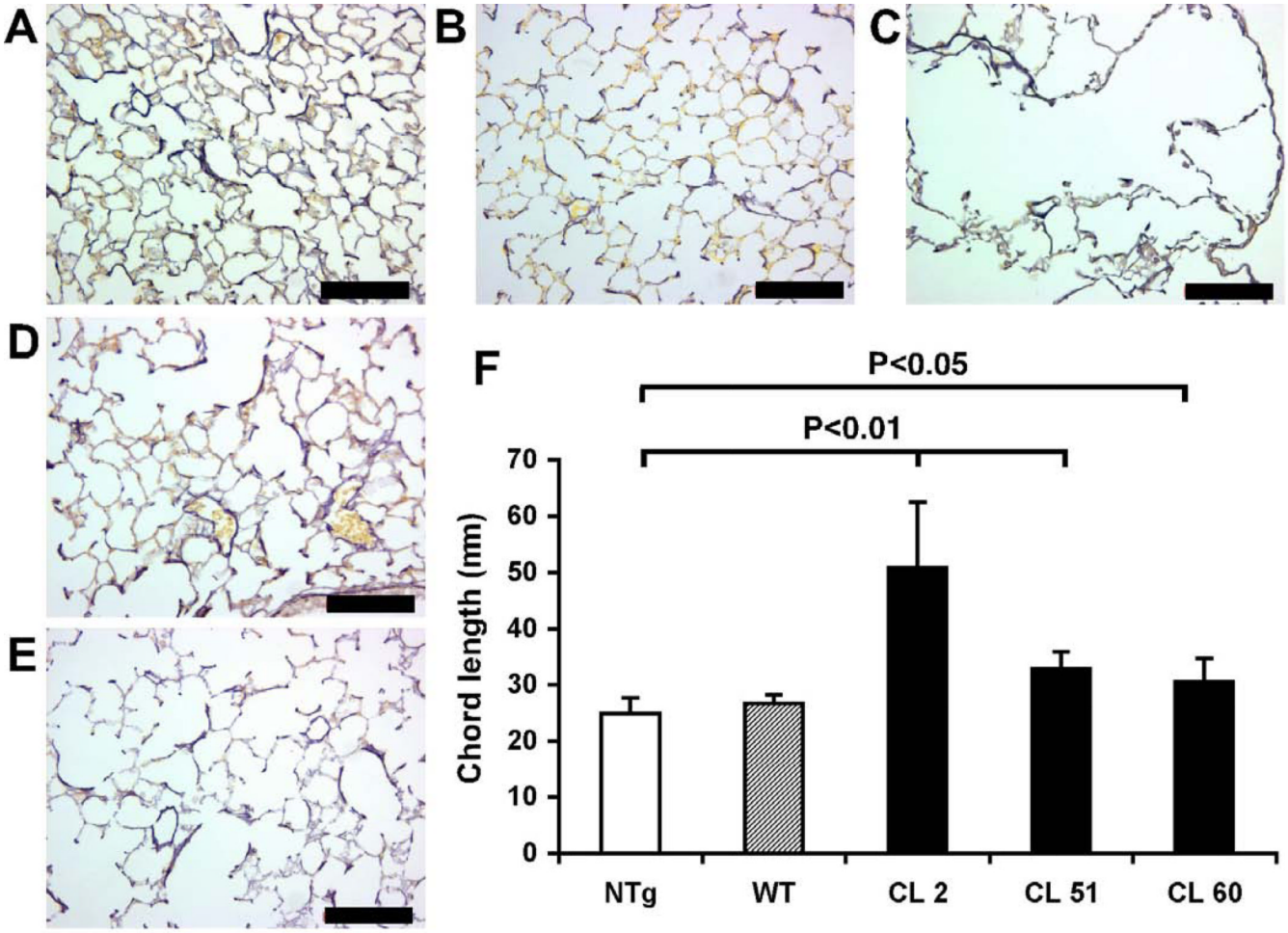

Figure 2. CL mice develop airspace enlargement

Whole lungs were inflated at constant pressure (20 cm H_2O), fixed, embedded in paraffin. Paraffin sections were stained for elastin using Hart's staining: (**A**) NTg, (**B**) WT, (**C**) CL line 2, (**D**) CL line 51, (**E**) CL line 60. Scale bars: 100μm. (**F**) Chord length measurements in lung sections were conducted using H&E stained sections. Transgenic lines with mutant elastin (CL, black bars) showed significantly increased chord length. Control mice with normal human elastin (WT, striped bar) did not show a significant increase. Error bars represent SEM. T-tests were used for statistical analysis.

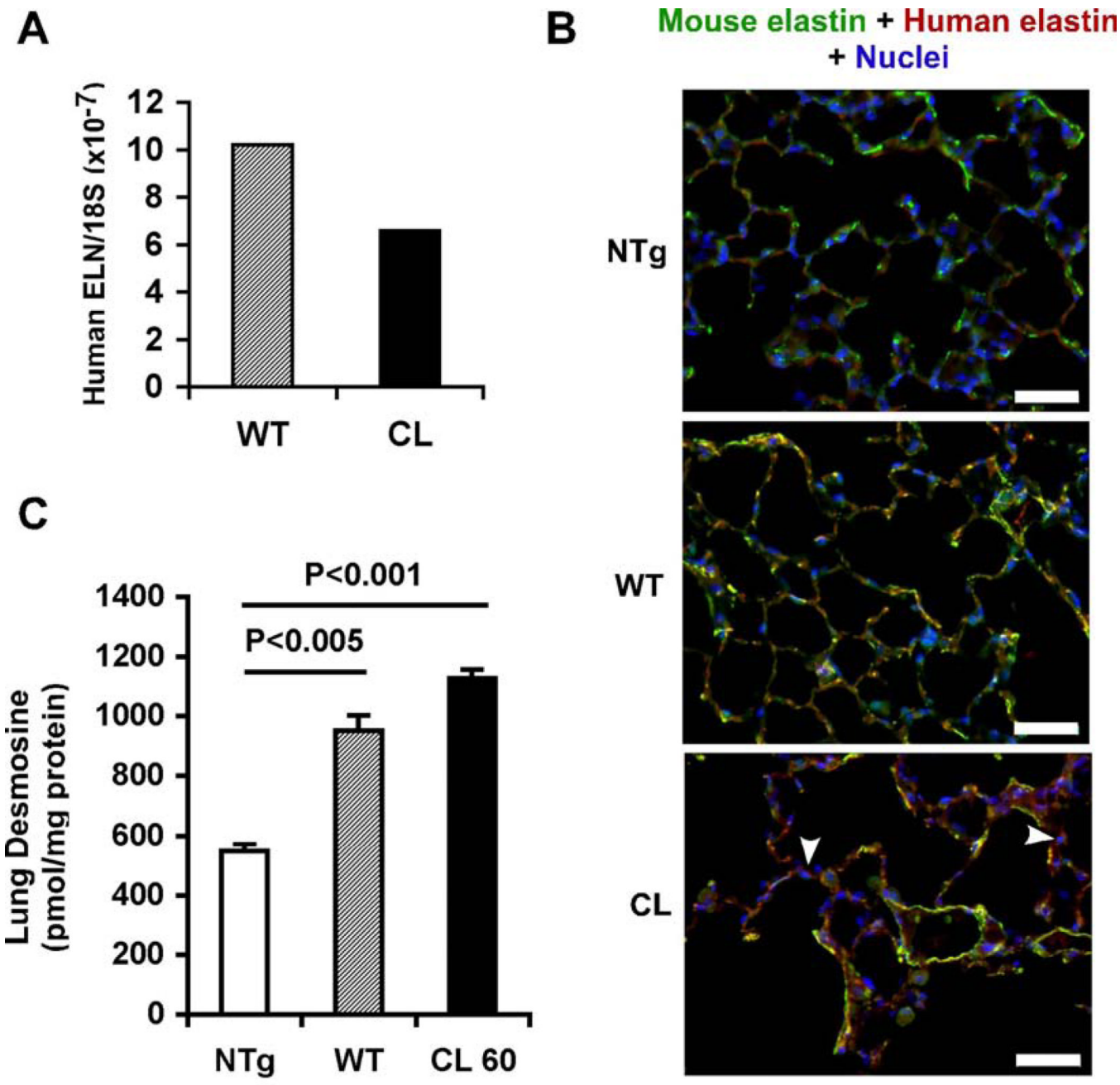

Figure 3. Transgenic elastin is incorporated into elastic fibers

(**A**) Transgene expression in lung was analyzed in WT and CL transgenic mice using real-time RT-PCR and absolute quantification. Final results were normalized by the copy number of 18s rRNA. (**B**) Colocalization of transgenic and endogenous elastin. Tissue sections of lung from NTg), control transgenic (WT), and mutant transgenic (CL) mice, were immunostained for mouse elastin (green), transgenic human elastin (red) and nuclei (blue). Merged images are shown. In addition to colocalization with mouse elastin in extracellular fibers (yellow), CL transgenic elastin also accumulated intracellularly (arrowheads). Scale bars: 50 μm. (**C**) Incorporation of transgenic human elastin into elastic fibers in mouse lung. Desmosine measurements in lungs from NTg, WT and CL mice (n=4, each group) were

normalized to total protein. Error bars represent SEM. T-tests were used for statistical analysis.

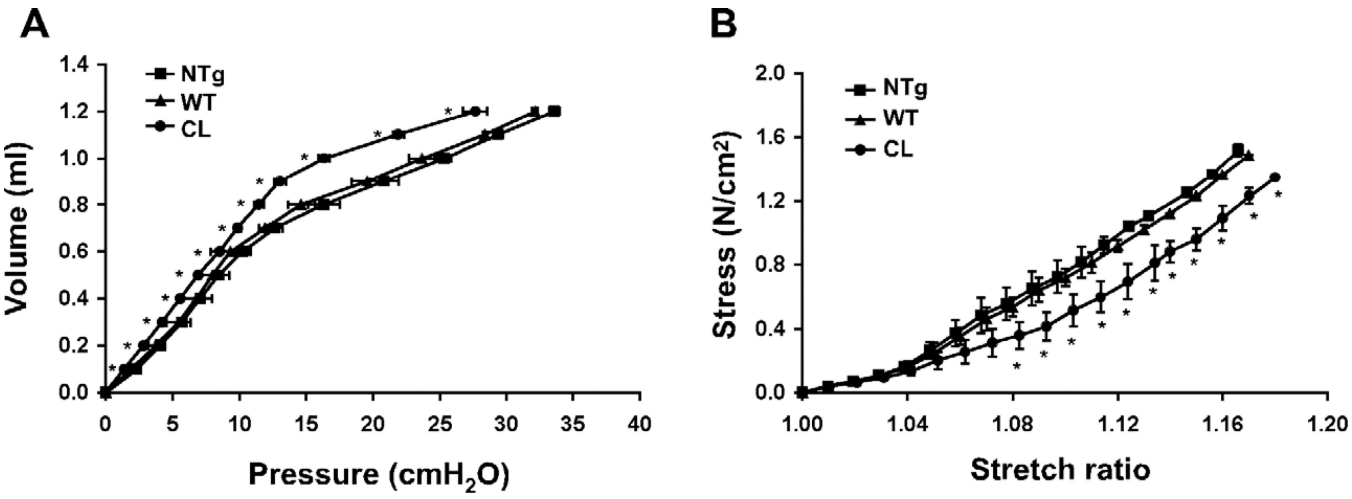

Figure 4. CL mutant elastin alters pulmonary mechanical properties

(**A**) Static pressure-volume curves were constructed by inflating *ex vivo* lungs from NTg, WT and CL mice in 0.1 ml increments, and measuring the resulting pressures. Expiratory curves are shown, n ≥ 5 mice per group. (**B**) Stress-strain curves were obtained by stretching isolated lung tissue strips from NTg, WT and CL lungs in 20 μm increments, and measuring the resulting forces; n ≥ 5 mice per group. Error bars represent SEM. Statistical analyses were conducted using t-tests, *$p<0.05$.

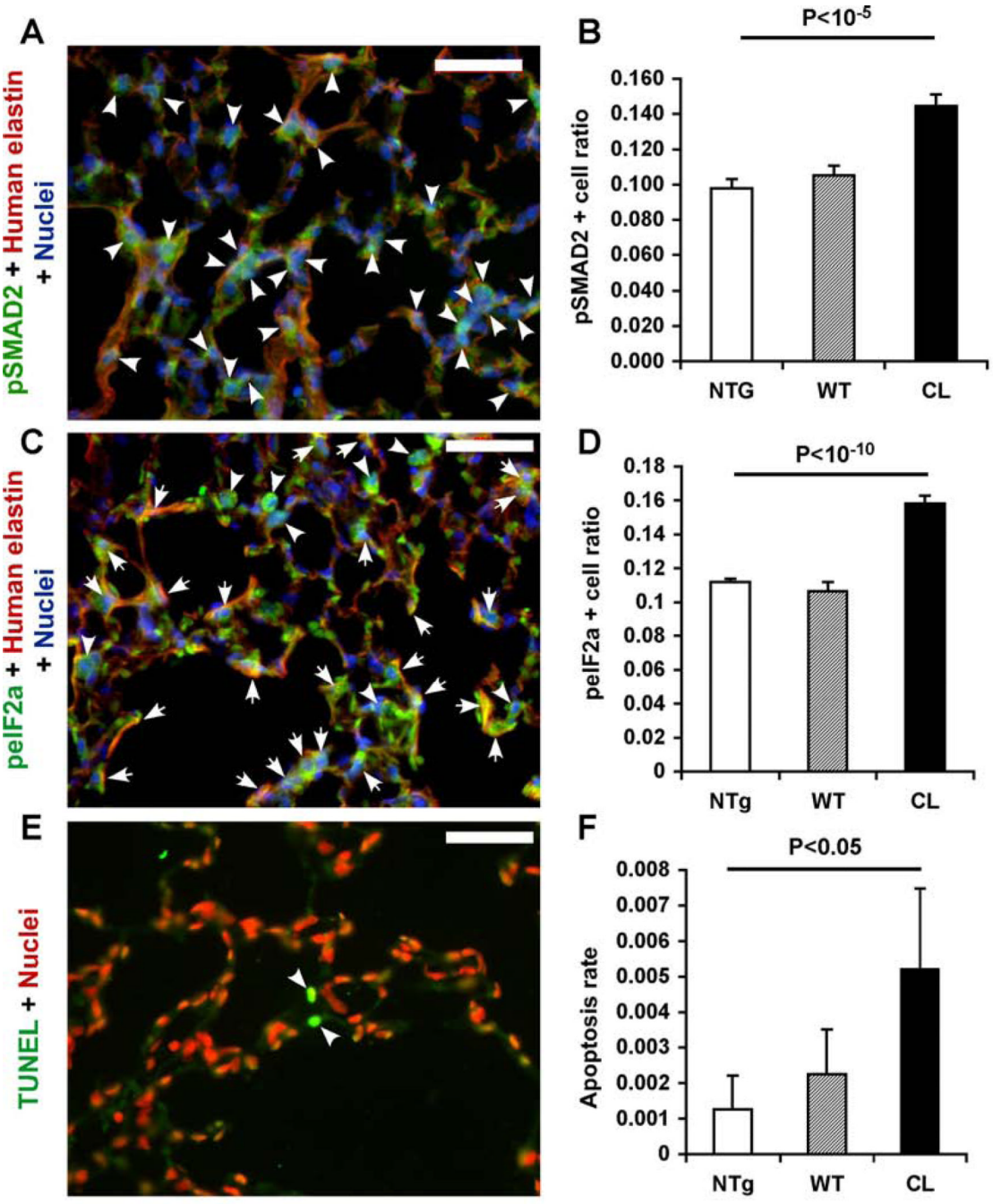

Figure 5. Increased TGFβ signaling, UPR and apoptosis in CL mice

(**A**) Representative merged micrograph of a lung section from a CL mouse stained for pSMAD2 (green), transgenic elastin (red), and nuclei (blue); pSMAD2-positive nuclei are indicated by arrowheads. Scale bar: 20μm. (**B**) Quantitative analysis of the ratio of pSMAD2-positive nuclei to the total number of nuclei. Error bars represent SEM. T-tests were used for statistical analysis. (**C**) Representative merged micrograph of a lung section from a CL mouse stained for peIF2a (green), transgenic elastin (red), and nuclei (blue); peIF2a -positive cells are indicated by arrowheads. Cells positive for both peIF2a and transgenic elastin are shown by arrows. Scale bar: 20μm. (**D**) Quantitative analysis of the

ratio of peIF2a -positive cells to the total number of cells. Error bars represent SEM. T-tests were used for statistical analysis. (**E**) Representative merged micrograph of a lung section from a CL mouse stained for apoptotic nuclei by TUNEL (green). Nuclei were counterstained by propidium iodide (red). Apoptotic nuclei are indicated by arrowheads. Scale bar: 20μm. (**D**) Quantitative analysis of the ratio of apoptotic nuclei to the total number of nuclei. Error bars represent SEM. Fisher's exact test was used for statistical analysis.